

THERMAL ANALYSIS OF COAL UNDER CONDITIONS OF RAPID HEATING

Hyok B. Kwon

Department of Environmental Protection, Kyungnam University
449 Wolyoung-Dong, Hapcho-Ku, Masan, 631-701 KOREA

and

Francis J. Vastola

Department of Materials Science and Engineering
Pennsylvania State University, University Park, PA 16802

Keywords: coal, pyrolysis, thermophysical property

INTRODUCTION

The heat effects of coal pyrolysis can be defined in terms of the sensible heats of the reacting substance and the heats of reaction. The heat capacities of coals and chars, necessary to evaluate the sensible heat contributions, have been measured by a variety of experimental techniques and the early published data have been reviewed (1, 2). However, the heat effects of pyrolysis have been the subject of considerable debate. Some investigators (3, 4) found that the pyrolysis was endothermic, while others (5-8) found it to be of an exothermic process. Temperature dependence (9) and rank dependence (10) of pyrolysis energetics add more complexities to the heat effects of pyrolysis processes.

Thermophysical properties such as the pyroheat, pyroheat capacity, and heat of pyrolysis of coal are important energetic data in design computations relating to various coal utilization processes. The most important use of thermophysical properties is in heat balance calculations. In general, the temperature of sufficiently small particles (say, 200 μm) during pyrolysis is assumed to be similar to that of the surrounding environment due to rapid heat transfer. Therefore, heat transfer does not influence the weight loss. And in most of the models used to predict the heat transfer effects, the net heat of pyrolysis is ignored. Freihaut and co-workers (11) incorporated heats of reaction in their model and predicted transport limitations for particle diameters below 100 μm . The endothermic heat effects during rapid pyrolysis have been identified (12, 13) qualitatively.

The objectives of this study were to measure the thermophysical properties of coal under conditions of rapid heating.

EXPERIMENTAL

Apparatus. A schematic diagram of the system used in this work is presented in Figure 1. Details of the apparatus and procedure are given elsewhere (14). The main components of the calorimeter are the grid reactor, electrical system, and microcomputer. The microcomputer is coupled with the reactor through a voltage regulator and a multiplexed analog/digital (A/D) converter for process control and data acquisition.

Electrical Heating. The reactor is an SS (Type 315) grid which is electrically heated by a constant voltage power supply. Heating rates were controlled by an adjustable voltage regulator powered by an acid-lead battery. The low internal resistance batteries and regulator ensure constant voltage at high current. The SS mesh grid and a brass bar, used as a reference resistance, make up the heating circuit (Figure 2). The low resistance (5.17 m Ω) and large mass (50 g) of the reference resistor minimize the changes in resistance from the variation in temperature due to resistive heating. Therefore, the reference resistance can be assumed to be constant during the experiment. The temperature of the reactor is monitored by a thermocouple spot-welded to the grid. For a given constant voltage the grid temperature reaches a steady state at which the resistive heat input balances losses by heat transfer. After being held at the final steady state temperature for the desired time, the sample is cooled by turning the power off. While the cooling period may last for a

few seconds, after the first 100 ms or so, the temperature becomes too low for pyrolysis reactions to continue (Figure 3).

Temperature Measurement. The pyrolysis temperature, defined as the temperature at the middle of the grid, is determined from a thin (50 μm) chromel-alumel thermocouple. The uncertainty in the actual temperature of the sample is reduced by use of a sample holder which contains a thermocouple as an integral part. A spot-weld fixes the junction just outside the folded grid near its center. Interaction between the heater and thermoelectric circuits at the mesh can cause gross distortions of the temperature signal and must be avoided. In this experiment, the thermoelectric circuits are isolated from the heating circuit by a differential input instrumentation amplifier.

Process Control and Data Acquisition. The system consists of an Apple II+ microcomputer and an 8-bit multiplexed A/D converter. The computer communicates with the system in two modes. First, the computer initiates and terminates the heating. Secondly, the computer monitors the change in the total voltage, the voltage across the reference resistor, and the thermocouple emf.

Calibration. A number of substances (Sn, Zn, Al; Aldrich Chemical Co., 5N) undergoing phase transitions at temperatures up to 933 K were tested (Table I). Temperature calibration was carried out using melting temperatures of these materials. At the same time, calorimetric calibration was carried out by using the enthalpies of fusion of these substances at their melting temperatures. The interval of the discontinuity corresponds to the enthalpy change (Figure 4). According to the calibration, the system overestimated the enthalpy change up to 19%, with 10% precision. The most probable reason for this overestimation is the underestimation of the heat loss of the grid. If the small metal sample is localized near the center of the grid employed, there will be a temperature difference through the grid, especially during the metal transition period. During this period, the transition tends to hold the grid temperature constant near its contact, while the temperature of the remainder of the grid increases. Since the temperature of the grid is monitored by the spot-welded thermocouple at the middle of the grid, its measured temperature underestimates the grid temperature and results in the undercompensation of heat loss, which is a strong function of temperature. This consideration is amply supported by experiment. If a small sample is located at the center of the grid, a three to five times greater experimental value than the literature value is obtained. However, when larger samples are spread over a larger area of the grid, this effect is markedly reduced. Moreover, this effect is markedly reduced both by the small particle size (140 x 170 mesh) and large mass (about 8 mg) of the coal used and by the less abrupt and more gradual coal pyrolysis reactions as contrasted with the sharp phase transition of a metal.

Sample Selection. Coal samples were obtained from the Penn State coal sample bank. Proximate and ultimate analyses of the coals are provided by the Penn State coal database and are presented in Table II.

Experimental Conditions. Experimental conditions are listed below:

- | | |
|------------------------------|---|
| 1. Sample size | 8.0 \pm 0.2 mg |
| 2. Particle size | 100 microns (140 x 170 mesh) |
| 3. Drying | Vacuum dry overnight at 383 K
and in situ for 5 min at 393 K |
| 4. Duration of reaction | 20 sec |
| 5. Final temperature | 880 \pm 5 K |
| 6. Heating rate | 200 K/s at 1 sec |
| 7. Soaking time | 15 sec |
| 8. Data acquisition interval | 20 ms |

Procedure. After a thermocouple was welded to a new mesh, which was folded into a "sandwich" heating element, forming a 2.5 x 12 mm strip and connected across the electrodes, the cell was evacuated, charged with nitrogen gas, and pre-fired to prevent further physical and chemical change

of the mesh. During the preheating, the mesh expanded and annealed until it reached a steady state condition. Then, 5 to 10 mg of coal sample was loaded into the mesh. The particles had a uniform diameter of approximately 100 μm (140 x 170 US mesh). This size was easily contained in the mesh with its 60- μm openings. After the coal was loaded, the cell was charged with nitrogen gas. The coal was dried inside the reactor for 10 min at 393 K. Next, the coal-grid system was heated with a constant voltage pulse, then cooled via simple heat dissipation. Subsequently, the remaining grid-char runs were made.

Data Reduction. In order to derive the thermal properties from the raw data, it is necessary to follow the reduction procedure which is described below and graphed in Figure 5. The interpretation of each symbol is given in Table III. Figure 2 shows the equivalent electrical circuit of the reactor. By measuring at 20-ms intervals, the two voltages e_s , e_r , and e_w , the temperature of the system can be measured and the power input to the system, W_i can be calculated,

$$W_i = \frac{e_s e_r}{R_s} \quad [1]$$

versus time. The power loss from the system at a given temperature can be calculated by determining the convective and radiative heat loss versus temperature according to the expression

$$W_l = A(T_s - T_{rm}) + B(T_s^4 - T_{rm}^4) \quad [2]$$

The terms A and B can be obtained experimentally at the end of a char run by heating the system to a series of temperatures and fitting the data to Equation 2 using an iterative technique. A check can be made to ascertain whether the radiation coefficient, B, is physically valid or not by comparing emissivity. Since the Stefan-Boltzmann law also can be applied to grey bodies, emissivity is the ratio of the radiation density of a surface to that of a black body at the same temperature.

$$\begin{aligned} \epsilon &= \frac{\text{energy actually radiated by the system}}{\text{energy radiated if the system were black}} \\ &= \frac{\text{evaluated radiant energy}}{\text{radiant energy black body}} \\ &= \frac{B(T_s^4 - T_{rm}^4)}{S(T_s^4 - T_{rm}^4)\sigma} \\ &= \frac{B}{S\sigma} \end{aligned} \quad [3]$$

The calculated emissivities (Table IV) from the evaluated radiation coefficients using Equation 3 are in good agreement with literature values (oxidized metals = 0.6 - 0.85; carbon, lampblack = 0.95¹⁸). By being able to measure the power input to the system versus time and temperature and by being able to calculate the power loss from the system versus temperature, net power absorbed by the system versus time can be calculated. From these values the integral of heat absorbed by the system versus time can be obtained. Each run would consist of three heatings, the grid alone, the coal sample in the grid, and finally the char remaining in the grid. By being able to normalize the runs to power absorbed versus temperature, the net heat absorbed by the grid, coal, and char is obtained (Figure 5d). The subtraction of the heat absorbed by the grid from that of the coal and the char runs enables the net heat requirements for heating the coal and the char to the final temperature to be obtained. The heat of pyrolysis is arrived at by subtracting the net heat absorbed by the char from that of the coal (Figure 5e). The differential of these values is shown in Figure 5f. The data are presented on the basis of the original mass of the coal sample.

RESULTS AND DISCUSSION

The thermophysical properties measured were 1) pyroheat, ΔH_p , which is the energy required to heat coal to a given temperature and is the sum of the heat of pyrolysis and heat capacity over the heating temperature interval; 2) pyroheat capacity, C_{ph} , which is the pyroheat normalized over a differential temperature interval; 3) heat of pyrolysis, ΔH_{py} , which is the thermal difference between heating coal and char to the same final temperature; and 4) pyrolysis heat capacity, C_{py} , which is the heat of pyrolysis normalized over a differential temperature interval. The experimental results for the coal samples are presented in Tables V through VII.

Char. As can be seen in Table V, the heat capacity of the char increases from room temperature to approximately 700 K. Since these figures are based on the original mass basis, the reported pyroheat capacity will be inversely dependent upon the VM content of the original coal. PSOC 867, with the smallest amount of VM and hence the greatest amount of remaining char, has the highest reported pyroheat and pyroheat capacity.

Coal. As the coal is heated, the mass remaining will decrease as VM is lost from the system being heated. Since the thermal data are reported on an original mass basis, the VM loss would tend to decrease the apparent pyroheat capacity; however, Table VI shows that the measured pyroheat capacity increases to a maximum in the 650 to 700 K temperature region. This is due to the endothermic reactions that are taking place during the pyrolysis. As the pyrolysis rate approaches its maximum in this temperature region, a significant portion of the energy absorbed is due to the pyrolysis. At the highest heating temperature, the pyroheat capacity of the remaining sample is close to that of the second heating (char run), indicating little VM was released during the char heating.

Pyrolysis. The difference in the quantity of heat needed to heat coal and the char to the same final temperature is that necessary to bring the coal material that will decompose to its decomposition temperature plus the heat required for the endothermicity of the reaction. Figure 4e and Table VII show that this amounts to a significant portion of the energy required to heat the coal. The differential of ΔH_{py} , C_{py} can be seen to peak during the period of maximum pyrolysis and then decrease as the pyrolysis rate approaches a low value. It should be noted that the pyroheat capacities of coal measured in this study do not include the energy necessary to heat the VM once it has been released from that release temperature to the final heating temperature.

CONCLUSIONS

The pyrolysis process for all the coals studied in this investigation was endothermic over the temperature range from 298 to 875 K. The pyrolysis rate and consequently the maximum rate of energy absorption approaches its maximum for all the coals in the temperature range 650 to 700 K. As the pyrolysis rate approaches its maximum in this temperature region, a significant portion of the energy absorbed is due to the endothermic reactions that are taking place during the pyrolysis. The differential of ΔH_{py} shows the peak during the period of maximum pyrolysis and the decrease as the pyrolysis rate approaches a low value.

ACKNOWLEDGMENTS

This study was made possible by financial support from the Coal Cooperative Program at The Pennsylvania State University. The authors thank the Penn State Coal Sample Bank and Data Base for supplying the sample and the analysis of the coal used in this study.

REFERENCES

1. Badzioch, S. *BCURA Monthly Bull.* 1960, 24(11), 485-520.

2. Kirov, N.Y. *BCURA Monthly Bull.* **1965**, 29(2), 33-39.
3. Davis, J.D.; Place, P.B. *Ind. Eng. Chem.* **1924**, 16(6), 589-592.
4. Lopez-Peinado, A.J.; Tromp, P.J.J.; Moulijn, J.A. *Fuel* **1989**, 68, 999-1004.
5. Whitehead, W.L.; Breger, I.A. *Science* **1950**, 111, 279-281.
6. Berkowitz, N. *Fuel* **1957**, 36, 355-373.
7. Gold, P.I. *Thermochimica Acta* **1980**, 42, 135-152.
8. Elder, J.P.; Harris, M.B. *Fuel* **1984**, 63, 262-267.
9. Agroskin, A.A.; Goncharov, E.I. *Coke Chem. USSR* **1980**, 12, 15-18.
10. Mahajan, O.P.; Tomita, A.; Walker, P.L., Jr. *Fuel* **1976**, 55, 63-69.
11. Freihaut, J.D.; Leff, A.A.; Vastola, F.J. *Prepr. Am. Chem. Soc., Div. Fuel Chem.* **1977**, 22, 149-157.
12. Freihaut, J.D.; Zabielski, M.F.; Serry, D.J. *Prepr. Am. Chem. Soc., Div. Fuel Chem.* **1982**, 27, 89-98.
13. Morel, O.; Vastola, F.J. *Prepr. Am. Chem. Soc., Div. Fuel Chem.* **1984**, 29, 77-82.
14. Kwon, H.B. Ph.D. Thesis, The Pennsylvania State University, **1987**.
15. Weast, R.C. Ed., *CRC Handbook of Chemistry and Physics*; 64th ed., CRC Press: Boca Raton, Florida, **1983**; E-385.

Table I. Calibration

Standard Substance	Literature (15)		Measured	
	m.p.(K)	$\Delta H_{\text{fusion}}(\text{J/g})$	m.p.(K)	$\Delta H_{\text{fusion}}(\text{J/g})$
Sn	505.1	60.7	496	71
			496	67
			495	70
Zn	692.7	113.0	688	120
			690	127
			691	125
Al	933.5	396.0	928	414
			920	423
			932	450

Table II. Characteristics of Coal Used

PSOC No.	423	415	572	309	867
Apparent Rank	SUBB	SUBC	HVC	HVC	AN
Proximate Analysis (dry)					
% Moisture (as received)	24.1	31.0	3.5	10.1	3.8
% Ash	13.6	11.1	6.4	20.4	13.9
% Volatile Matter	50.5	50.6	52.6	37.6	3.7
% Fixed Carbon	35.9	38.3	41.1	42.0	82.4
Ultimate Analysis (daf)					
% C	72.6	72.5	73.1	77.1	95.1
% H	6.1	5.7	4.9	5.8	1.2
% N	1.1	1.4	0.0	1.7	0.8
% S (total)	2.0	0.9	0.3	1.0	0.6
% O (by difference)	18.1	19.4	21.7	14.4	2.3
Net Calorific Value (kJ/g, dmmf)	30.3	29.4	27.5	31.6	34.4

Table III. Data Reduction Symbols

<u>English Symbols</u>	
A	Coefficient for conduction and convection
B	Coefficient for radiation
e	Voltage drop
H	Enthalpy
I	Current
R	Resistance
T	Temperature
W	Power
<u>Subscripts</u>	
g	Grid
i	Input
l	Loss
r	Reference
s	System
rm	Room
tc	Thermocouple

Table IV. Calculated Emissivities^a

PSOC No.	Run No.	B ($\times 10^{12}$)	ϵ
423	830	5.372	0.65
415	780	5.465	0.66
572	680	6.960	0.84
309	790	6.485	0.78
867	1000	5.906	0.71

^a Measured surface area of grid, $1.46 \times 10^4 \text{ m}^2$;
 Calculated emissivity of black body; $\epsilon = 5.67 \times 10^8 \text{ W/m}^2\text{K}^4$.

Table V. Thermophysical Properties of Char

PSOC ID No.	423		415		572		309		867	
Temperature (K)	ΔH_{ph} (J/g)	C_{ph} (J/gK)								
400	35	0.52	30	0.51	13	0.48	24	0.48	41	0.74
425	52	0.63	50	0.63	28	0.61	38	0.59	63	0.89
450	69	0.73	64	0.75	46	0.74	56	0.69	92	1.04
475	89	0.83	88	0.87	66	0.87	72	0.79	121	1.18
500	112	0.92	110	0.98	91	0.98	96	0.87	159	1.30
525	138	1.00	138	1.08	121	1.08	121	0.96	191	1.42
550	165	1.08	167	1.16	151	1.19	151	1.04	226	1.51
575	194	1.15	201	1.24	184	1.29	174	1.11	269	1.60
600	221	1.20	235	1.31	213	1.37	201	1.19	313	1.69
625	257	1.25	265	1.37	250	1.44	236	1.26	356	1.77
650	291	1.30	306	1.42	293	1.48	269	1.34	403	1.84
675	323	1.33	340	1.45	333	1.52	302	1.42	445	1.90
700	357	1.34	376	1.47	370	1.56	337	1.49	502	1.93
725	392	1.34	416	1.47	411	1.58	377	1.54	553	1.94
750	429	1.34	458	1.47	448	1.59	419	1.58	605	1.94
775	465	1.33	492	1.46	490	1.60	464	1.61	652	1.94
800	496	1.32	530	1.46	534	1.60	506	1.62	701	1.93
825	524	1.32	566	1.45	573	1.60	542	1.63	742	1.93
850	552	1.32	595	1.45	612	1.60	578	1.64	783	1.93
875	578	1.32	623	1.45	649	1.60	614	1.64	825	1.93

Table VI. Thermophysical Properties of Coal

PSOC ID No.	423		415		572		309		867	
Temperature (K)	ΔH_{ph} (J/g)	C_{ph} (J/gK)								
400	43	0.81	41	0.75	20	0.64	33	0.71	46	0.76
425	68	1.00	57	0.95	36	0.82	55	0.88	70	0.91
450	101	1.18	84	1.15	63	1.01	80	1.04	96	1.06
475	133	1.35	121	1.34	93	1.19	110	1.18	126	1.20
500	172	1.51	160	1.52	123	1.37	145	1.32	160	1.33
525	212	1.65	205	1.67	164	1.54	182	1.44	196	1.45
550	259	1.77	253	1.82	207	1.70	222	1.56	235	1.55
575	307	1.86	293	1.94	255	1.84	263	1.68	276	1.65
600	355	1.95	352	2.05	301	1.96	305	1.79	322	1.74
625	410	2.02	403	2.13	356	2.06	352	1.89	367	1.82
650	462	2.07	463	2.20	411	2.14	403	1.97	414	1.89
675	513	2.09	521	2.24	468	2.20	456	2.03	464	1.94
700	571	2.06	576	2.22	526	2.22	508	2.06	514	1.97
725	628	1.98	636	2.14	583	2.21	566	2.00	566	1.97
750	678	1.83	697	1.97	644	2.10	620	1.87	619	1.96
775	729	1.67	755	1.79	702	1.93	674	1.76	670	1.94
800	772	1.56	799	1.66	754	1.79	721	1.70	717	1.93
825	805	1.49	834	1.59	803	1.71	763	1.66	761	1.93
850	838	1.46	863	1.55	839	1.66	798	1.65	804	1.92
875	864	1.45	892	1.54	876	1.64	834	1.65	846	1.92

Table VII. Thermophysical Properties of Pyrolysis

PSOC ID No.	423		415		572		309		867	
Temperature (K)	ΔH_{ph} (J/g)	C_{ph} (J/gK)								
400	8	0.26	10	0.22	6	0.15	9	0.22	5	0.02
425	15	0.35	7	0.30	7	0.20	16	0.28	7	0.02
450	32	0.43	19	0.39	17	0.26	24	0.33	4	0.02
475	43	0.51	32	0.46	27	0.32	37	0.39	4	0.02
500	59	0.58	49	0.52	31	0.38	49	0.43	0	0.03
525	74	0.64	67	0.58	42	0.45	61	0.47	4	0.03
550	94	0.68	85	0.64	56	0.50	71	0.51	9	0.04
575	112	0.71	92	0.69	70	0.54	88	0.55	7	0.05
600	133	0.74	116	0.73	87	0.58	103	0.59	8	0.05
625	152	0.76	138	0.76	105	0.61	116	0.62	10	0.05
650	171	0.77	156	0.78	118	0.65	133	0.63	10	0.05
675	189	0.76	180	0.79	134	0.67	154	0.62	19	0.04
700	214	0.73	199	0.76	156	0.67	170	0.58	11	0.03
725	236	0.66	219	0.69	171	0.64	189	0.48	12	0.03
750	248	0.52	239	0.54	195	0.53	200	0.32	14	0.02
775	264	0.37	263	0.37	211	0.37	209	0.19	17	0.01
800	276	0.26	268	0.23	220	0.22	214	0.09	16	0.00
825	281	0.19	268	0.15	229	0.12	221	0.04	18	0.00
850	285	0.15	268	0.11	227	0.07	220	0.02	20	0.00
875	286	0.14	269	0.09	227	0.05	220	0.02	21	0.00

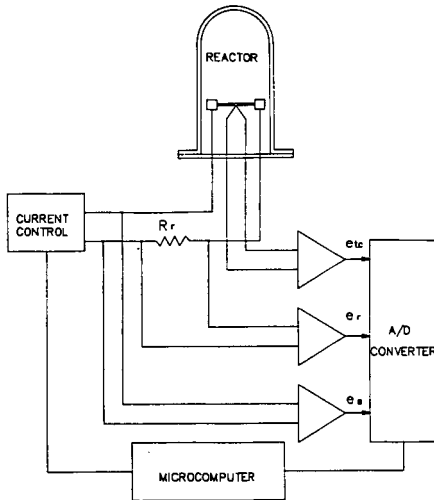


Figure 1. Schematic diagram of the system.

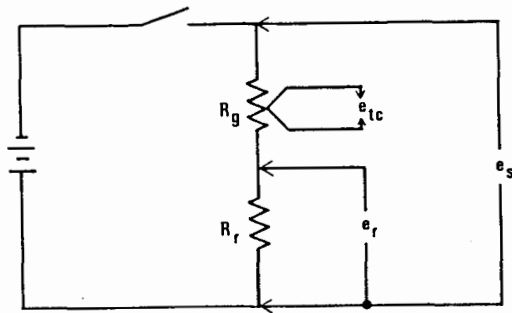


Figure 2. Equivalent circuit of the heating system.

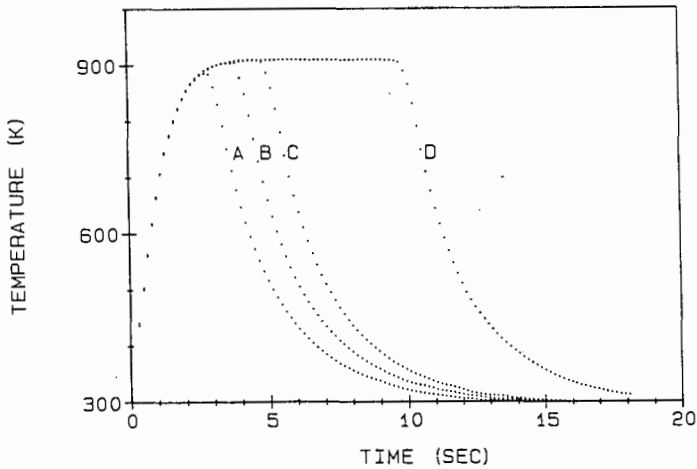


Figure 3. Heating and cooling curves for blank grid. Soak time at final temperature (sec.); 0 (A), 1 (B), 2 (C), and 7 (D).

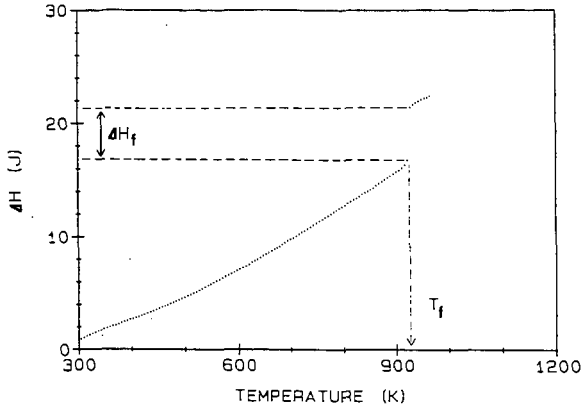


Figure 4. Typical calibration run for aluminum.

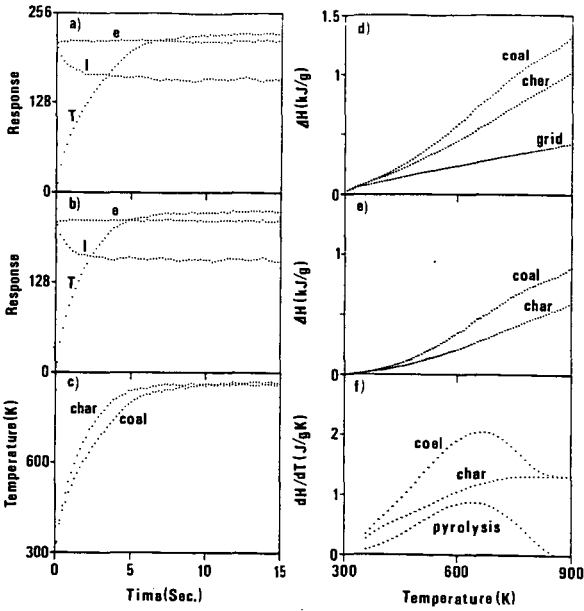


Figure 5. Data reduction. Coal run (a), char run (b), temperature profile (c), enthalpy change (d), normalized enthalpy change (e), and rate of enthalpy change (f).